

Control of Dzyaloshinskii-Moriya interaction in $\text{Mn}_{1-x}\text{Fe}_x\text{Ge}$: a first-principles study

Takashi Koretsune,¹ Naoto Nagaosa,^{1,2} and Ryotaro Arita¹

¹RIKEN Center for Emergent Matter Science (CEMS), Wako, Saitama 351-0198, Japan

²Department of Applied Physics, University of Tokyo, Hongo, Tokyo 113-8656, Japan

(Dated: August 2, 2021)

Motivated by the recent experiment on the size and helicity control of skyrmions in $\text{Mn}_{1-x}\text{Fe}_x\text{Ge}$ [K. Shibata et al., *Nature Nanotechnology* **8**, 732 (2013)], we study how the Dzyaloshinskii-Moriya (DM) interaction changes its size and sign in metallic helimagnets. By means of first-principles calculations, we successfully reproduce the non-trivial sign change of the DM interaction observed in the experiment. While the DM interaction sensitively depends on the carrier density or the detail of the electronic structure such as the size of the exchange splitting, its behavior can be systematically understood in terms of the distribution of anticrossing points in the band structure. By following this guiding principle, we can even induce gigantic anisotropy in the DM interaction by applying a strain to the system. These results pave the new way for skyrmion crystal engineering in metallic helimagnets.

A skyrmion is a topologically protected nano-size spin texture found in several magnets¹⁻⁵. Due to its unusual spin structure, many intriguing behaviors such as topological Hall effects, current-driven motion, and multiferroic behavior have been observed⁶. Although there is a huge potential to design novel functional materials by exploiting these unique electromagnetic properties, skyrmion engineering or skyrmion-crystal engineering is yet to be established. Here, the key issue is how to manipulate the size and helicity of skyrmions. Regarding this problem, a recent experiment for the representative skyrmion system $\text{Mn}_{1-x}\text{Fe}_x\text{Ge}$ has shown that we can tune the skyrmion size and helicity by changing the carrier density^{7,8}.

The Hamiltonian which determines the nature of skyrmions is

$$H = \int dr \left[\frac{J}{2} (\nabla M)^2 + DM \cdot (\nabla \times M) \right], \quad (1)$$

where M is the magnetization per volume, D is the Dzyaloshinskii-Moriya (DM) interaction coefficient and J is the ferromagnetic exchange coupling, respectively. For materials design of skyrmion crystals, we need to know the precise value of D/J . However, non-empirical evaluation of these parameters in the classical continuum model has been a difficult challenge, since it requires an elaborate multi-scale approach spanning the quantum to classical regime. For the insulating skyrmion system Cu_2OSeO_3 ⁹, there is a work in which the spin Hamiltonian (1) was derived from first principles¹⁰. By comparing the total energy of various magnetic states, they determined the value of D/J , and succeeded in reproducing the experimentally measured skyrmion size. However, the guiding principle to control the values of D/J is yet to be obtained.

On the other hand, for metallic systems, the situation is different. There are several studies for the estimate of D ¹¹⁻²⁰. Among them, recently, one of the present authors (NN) and his collaborators have shown that the DM interaction in the two-band model drastically changes when the band anticrossing point resides near the Fermi level²⁰. The story is analogous to that of anomalous Hall conductivity, in which the band anticrossings act as magnetic monopoles in momentum

space²¹. In Ref. 19, a Berry phase expression for the DM interaction has also been formulated. These studies stimulate us to explore a fascinating possibility of controlling the DM interaction in metallic systems by manipulating the electronic structure. Indeed, the fact that not only the size but also the helicity of skyrmions in $\text{Mn}_{1-x}\text{Fe}_x\text{Ge}$ changes as a function of x indicates that we have a good chance to control the value of D .

In this paper, we show a quantitative analysis of the DM interaction in the metallic helimagnet, $\text{Mn}_{1-x}\text{Fe}_x\text{Ge}$, based on *ab initio* density-functional theory (DFT) calculation. From the obtained band structure, we evaluate the off-diagonal spin susceptibility which is a direct measure of the DM interaction. We find that the sign change of D observed in the experiment for $\text{Mn}_{1-x}\text{Fe}_x\text{Ge}$ is successfully reproduced. The carrier-density dependence of D can be systematically understood in terms of the distribution of band anti-crossing points in the electronic structure. We demonstrate that the sign and the size of D can be controlled as a function of the carrier density or the size of the exchange splitting. There is also an interesting possibility to induce gigantic anisotropy in D by applying a strain to the system.

Results

DM interaction in the continuum model. Let us first look at the second term in the Hamiltonian (1). This indicates that q -linear term in the spin susceptibility, $\chi^{\alpha\beta}$, should be proportional to the DM interaction coefficient, D . Therefore, to estimate D in the continuum limit from the DFT calculation, we compute the long-wave length limit of the spin susceptibility, that is,

$$\tilde{D}_\beta \equiv \lim_{q \rightarrow 0} \frac{\partial \chi^{\alpha\gamma}(\mathbf{q}, i\omega_n = 0)}{i\partial q^\beta}. \quad (2)$$

Here, $(\alpha, \beta, \gamma) = (x, y, z), (y, z, x),$ or (z, x, y) and \tilde{D}_β corresponds to the coefficient for $M_\alpha \partial M_\gamma / \partial \beta$ in Eq. (1). Since we consider the skyrmions in the x - y plane under the total magnetic moment along the z -axis, hereafter we focus on \tilde{D}_x and \tilde{D}_y . In Eq. (2), we use the non-interacting spin suscepti-

bility defined as

$$\chi_0^{\alpha\gamma}(\mathbf{q}, i\omega_l) = -\frac{T}{V} \sum_{l, l', s_1, s_2, s_3, s_4} \sum_{\mathbf{k}, m} \sigma_{s_4 s_1}^\alpha \times G_{l s_1 l' s_2}^0(\mathbf{k}, i\omega_m) \sigma_{s_2 s_3}^\gamma G_{l' s_3 l s_4}^0(\mathbf{k} + \mathbf{q}, i\omega_m + i\omega_l) \quad (3)$$

where, σ is the Pauli matrix and G^0 is the non-interacting Green's function in the orbital basis. Using this non-interacting spin susceptibility, we can write as $\tilde{D}_\beta = (1/V) \sum_{\mathbf{k}} \tilde{D}_\beta(\mathbf{k})$ with

$$\tilde{D}_\beta(\mathbf{k}) = \lim_{\mathbf{q} \rightarrow 0} \frac{\partial}{i\partial q_\beta} \sum_{n, n'} \frac{f(\varepsilon_{n'\mathbf{k}+\mathbf{q}}) - f(\varepsilon_{n\mathbf{k}})}{\varepsilon_{n'\mathbf{k}+\mathbf{q}} - \varepsilon_{n\mathbf{k}}} \times \langle n\mathbf{k} | \sigma^\alpha | n'\mathbf{k} + \mathbf{q} \rangle \langle n'\mathbf{k} + \mathbf{q} | \sigma^\gamma | n\mathbf{k} \rangle, \quad (4)$$

where $|n\mathbf{k}\rangle$ is the eigenvector of the Kohn-Sham Hamiltonian with the eigenvalue of $\varepsilon_{n\mathbf{k}}$. Hence, we can discuss the DM interaction in terms of the band structure. Although there is a sophisticated approach to compute D ¹⁹, we employ the current simple approach to explore various parameters and materials. Furthermore, this approach is appropriate to obtain a guiding principle for controlling D as discussed below.

Ab initio band structure. Figure 1(a) shows the DFT band structure of FeGe (black solid lines). Here, we include the spin-orbit couplings and assume the ferromagnetic moment along the z axis. The calculated local magnetic moment is $1.18 \mu_B$ per Fe atom, which is consistent with the experiments^{22,23} and previous calculations²⁴. Using this electronic structure, we construct the tight-binding model made of Fe 3d and Ge 4p Wannier orbitals to reproduce the band structure below the Fermi level as shown in red broken lines. The densities of states for up spin (red line) and down spin (blue line) are also shown in Fig. 1(a). As can be seen, there is a large exchange splitting, Δ . According to the energy difference of up and down spins for the Fe 3d orbitals, we obtain $\Delta = 1.17$ eV. In Fig. 1(b), the obtained tight-binding band structure around the Fermi level is illustrated with colors representing the weight of the up spin. Since we consider ferromagnetic electronic structure, each band can be basically characterized as either up-spin or down-spin band as shown in Fig. 1(b). In addition, due to the spin-orbit couplings, there are several anticrossing points where complex spin texture emerges.

Ab initio evaluation of the DM interaction. Let us start with the simple two-band model in two dimensions considered in Ref. 20. The Hamiltonian is represented by a 2×2 matrix,

$$H = k_x \sigma^x + k_y \sigma^y + m \sigma^z. \quad (5)$$

We assume that the band dispersion is linear in the k_x - k_y plane, and dispersionless in the k_z direction. We introduce m to open a gap at the band crossing point as shown in Fig. 2 (a). The static spin susceptibility can be calculated analyti-

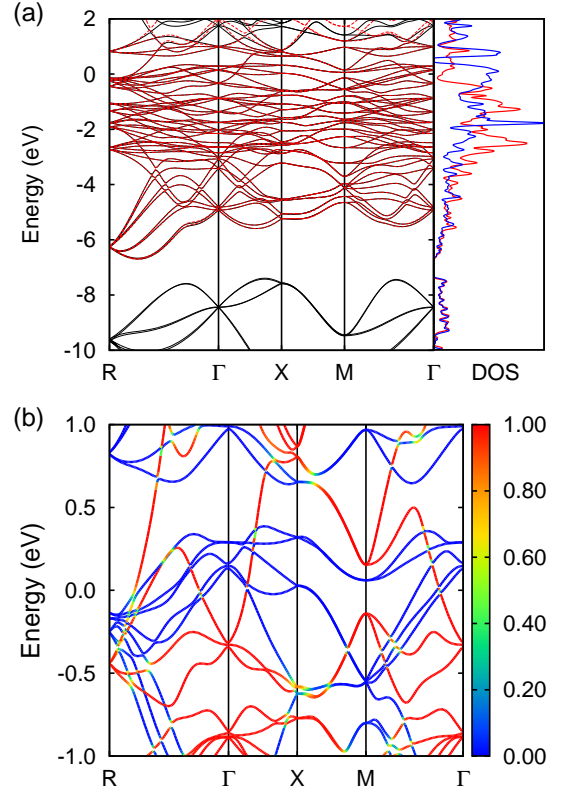


FIG. 1. **Band structure of FeGe.** (a) Comparison between DFT band structure (black solid lines) and tight-binding band structure (red broken lines). Densities of states for up spin (red line) and down spin (blue line) are also shown. (b) Detailed band structure around the Fermi level with colors representing the weight of the up spin; that is, red (blue) lines correspond to up-spin (down-spin) bands. The Fermi level is set to zero.

cally, and the result is

$$\begin{aligned} \tilde{D}_y &= \lim_{q \rightarrow 0} \frac{\partial \chi^{xz}}{\partial (iq^y)} = \frac{1}{V} \sum_{\mathbf{k}} \frac{\delta(\mu - E_{\mathbf{k}}) - \delta(\mu + E_{\mathbf{k}})}{4E_{\mathbf{k}}} \\ &= \frac{1}{8\pi} [\theta(\mu - m) - \theta(-\mu - m)] \quad (6) \end{aligned}$$

where μ is the chemical potential and $E_{\mathbf{k}} = \sqrt{k_x^2 + k_y^2 + m^2}$.

It is interesting to note that \tilde{D}_y is negative for $\mu < -m$, and positive for $\mu > m$ as shown Fig. 2 (b). If we reverse the spin texture by modifying the Hamiltonian as $\sigma_y \rightarrow -\sigma_y$, \tilde{D}_y becomes positive for $\mu < -m$, and negative for $\mu > m$. This result suggests that the position of the Fermi level and the spin texture around the anticrossing point are crucial to determine the sign of D .

In real materials, the situation is not so simple as that of this two-band model. The anticrossing points form complex surfaces in a four-dimensional space spanned by the energy and the wave number, and the electronic states around neighboring anticrossing points can hybridize with each other. In Fig. 2 (c), as a representative case, we schematically show how \tilde{D}

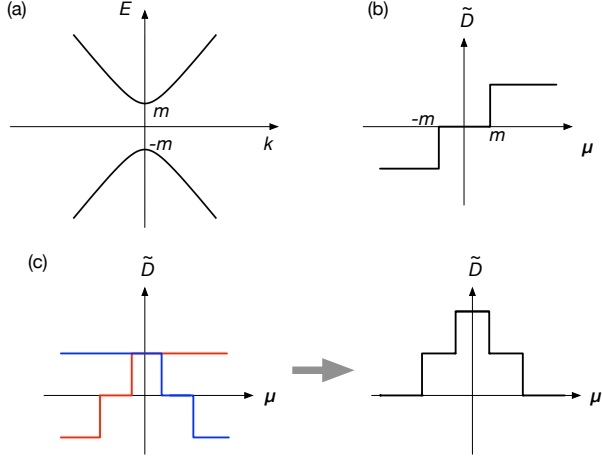


FIG. 2. **Schematic pictures of the DM interaction around the band anticrossing points.** (a) Band structure of the two-band model defined in Eq. (5) and (b) the chemical potential dependence of the DM interaction corresponding to this band structure. When two anticrossing points with different energies and spin textures with opposite chiralities reside close to each other, the peak structure appears as shown in (c).

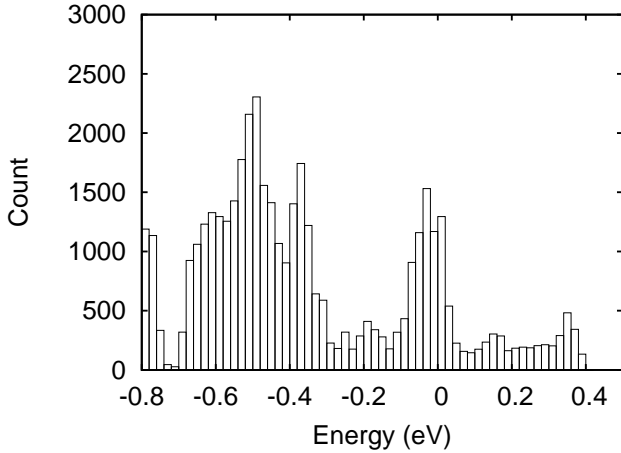


FIG. 3. **Distribution of anticrossing points.** Number of k points in $64 \times 64 \times 64$ mesh where the up-spin weight, w_{\uparrow} , satisfies $0.4 < w_{\uparrow} < 0.6$.

changes as a function of the chemical potential when two anticrossing points with different energies and spin textures with opposite chiralities reside close to each other. Thus, when many anticrossings are densely clustered around the Fermi level, the sign and the size of \tilde{D} should change drastically. In fact, the band structure of FeGe has many anticrossing points around the Fermi level (see Fig. 1). To visualize the distribution of the anticrossing points as a function of energy, in Fig. 3, we plot the number of k points in $64 \times 64 \times 64$ mesh where the up-spin weight, w_{\uparrow} , satisfies $0.4 < w_{\uparrow} < 0.6$. We can see that there are two peaks around $\mu = 0$ eV and -0.5 eV, where \tilde{D} is expected to change significantly.

To analyze the contribution of each anticrossing point, next,

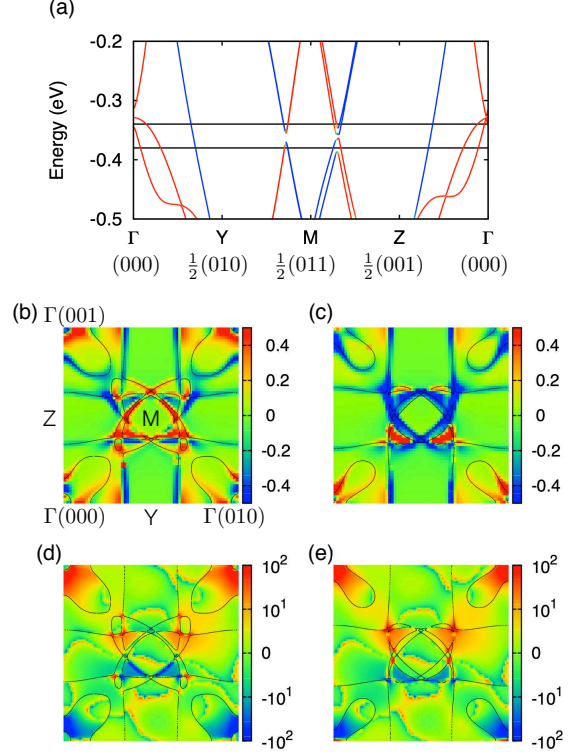


FIG. 4. **Contribution of anticrossing points to the DM interaction.** (a) Band structure around the anticrossing points and k -dependence of $\tilde{D}_x(\mathbf{k})$ at two different chemical potentials (b) $\mu = -0.38$ eV and (c) $\mu = -0.34$ eV at $T = 100$ K. Fermi surface is also shown in black lines. For comparison, the Berry curvatures at (d) $\mu = -0.38$ eV and (e) $\mu = -0.34$ eV are plotted.

we focus on the anticrossing points around the M ($0 \ 1/2 \ 1/2$) point. In Fig. 4(a), there are two anticrossing points between Y and M points, and between M and Z points. In $k_x = 0$ plane, such anticrossing points continuously form a closed loop around the M point. In Fig. 4(b) and (c), we show the k -dependence of $\tilde{D}_x(\mathbf{k})$ when the chemical potential is below and above the anticrossing points shown in black lines in Fig. 4(a), respectively. We see that the texture around the M point drastically changes when the chemical potential sweeps across the anticrossing points, which is consistent with the simple two-band calculation²⁰. Note that $\tilde{D}_x(\mathbf{k})$ around the other Fermi surfaces such as the one between Γ - Y line are not negligible although the spin mixture is not so significant. This is because the effect of spin mixing extends away from anticrossing points; that is, $\tilde{D}(\mathbf{k})$ has non-negligible values typically up to 0.2 - 0.3 eV away from anticrossing points. For comparison, in Fig. 4 (d) and (e), we show the Berry curvature, $\Omega^z(\mathbf{k})$, which is the origin of intrinsic anomalous Hall conductivity (AHC)^{21,25}. $\Omega^z(\mathbf{k})$ is defined as

$$\Omega^z(\mathbf{k}) = -\hbar^2 \sum_{n \neq n'} f(\varepsilon_{n\mathbf{k}}) \frac{2\text{Im}\langle n\mathbf{k}|v_x|n'\mathbf{k}\rangle \langle n'\mathbf{k}|v_y|n\mathbf{k}\rangle}{(\varepsilon_{n'\mathbf{k}} - \varepsilon_{n\mathbf{k}})^2}, \quad (7)$$

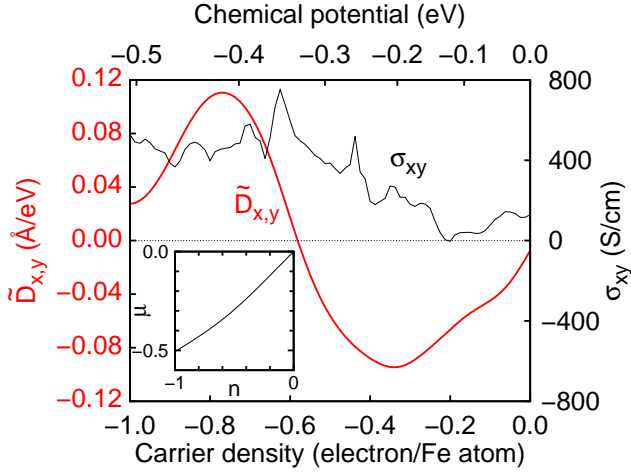


FIG. 5. **Carrier density dependence of the DM interaction.** DM interaction coefficients, \tilde{D}_x , and \tilde{D}_y , and the AHC, σ_{xy} as a function of the carrier density, n . The inset shows the relation between the chemical potential μ and carrier density n . We use the rigid band approximation starting from the electronic structure of FeGe ($n = 0.0$, $\mu = 0.0$ eV). $n = -1.0$ ($\mu = -0.506$ eV) corresponds to the carrier density of MnGe.

where v_x and v_y are velocity operators. Since the spin mixing is important for both cases, there are common regions where the contributions to the DM interaction and AHC are large. However, in the Berry curvature, the summation in Eq. (7) is restricted to $n \neq n'$ while it is not in Eq. (4). As a result, only the restricted region is important for AHC, which is in sharp contrast to \tilde{D} .

Figure 5 shows the resulting $\tilde{D}_{x,y}$ at $T = 300\text{K}$ as a function of the carrier density together with the AHC, σ_{xy} . In the calculation, we use the rigid band approximation. The relation between the carrier density, n , and the chemical potential, μ , is shown in the inset of Fig. 5. At $\mu = -0.506$ eV, the number of hole is 1.0 per Fe atom, which corresponds to the carrier density in MnGe. In Fig. 5, we find that $\tilde{D}_{x,y}$ shows clear sign change from FeGe ($\tilde{D}_{x,y} < 0$) to MnGe ($\tilde{D}_{x,y} > 0$), which is consistent with the experimental sign change of skyrmion helicity^{7,8}, and is in sharp contrast to σ_{xy} . The positive (negative) hump structure in $\tilde{D}(\mu)$ around $\mu \sim 0.4$ (0.2) eV originates from the peak structure around $\mu \sim 0.5$ (0.0) eV in Fig. 3, respectively. If we assume that contributions from $\mu \sim 0$ (-0.5) eV is negative (positive), we can understand why \tilde{D} changes its sign around $\mu \sim 0.3$ eV. As for σ_{xy} , the calculated value of σ_{xy} in MnGe is larger than that in FeGe and there is no sign change. This behavior including size and sign agrees well with the experimental anomalous Hall contribution to σ_{xy} for MnGe²⁶ and for $\text{Mn}_{1-x}\text{Fe}_x\text{Ge}$ ²⁷.

Strain-induced huge anisotropy of the DM interaction.

According to the above discussion, there are several ways to change the size and sign of D . As we have seen above, D can be efficiently controlled by carrier doping. We can

also exploit the temperature dependence of the exchange splitting. When the relative position of up- and down- spin band changes, the distribution of anticrossing points in the band structure also changes, which will have a direct impact on D . As an example, we will show later the change in $\tilde{D}_{x,y}$ of FeGe as a function of the moment per Fe atom in Fig. 8 (b). This mechanism can be related to the temperature dependence of the magnetic moment and skyrmion size in MnGe²⁶. Another interesting possibility is to make use of the strain effect. If we apply a strain to the system, the symmetry of the electronic structure can be lowered, and the distribution of the anticrossing points will change drastically. This effect is expected to be prominent especially when D changes its sign. Figure 6 (a) shows the calculated $\tilde{D}_{x,y}$ at $n = -0.45$ for which we apply the uniaxial strain along the y direction. We find that the difference between \tilde{D}_x and \tilde{D}_y actually enhances particularly by the elongation along the y axis; \tilde{D}_x is about 40 % (400 %) larger than \tilde{D}_y at +2 % (+5%) strain. The carrier density dependence of the anisotropy, $|\tilde{D}_y/\tilde{D}_x|$, for fixed strain of +5% is shown in Fig. 6 (b). We can see that the anisotropy becomes large particularly around the region of sign change.

Discussion

In the present calculation, we employed the rigid band approximation. To examine its validity, we have performed a calculation for the other end material MnGe and doped negative carriers by the rigid band approximation. As shown in Fig. 7, we have obtained a qualitatively similar result in that \tilde{D} is positive (negative) for the end material MnGe (FeGe). Thus the result that \tilde{D} for $\text{Mn}_{1-x}\text{Fe}_x\text{Ge}$ changes its sign between $x = 0$ and 1 should be robust, even when we go beyond the rigid band approximation.

Regarding the crystal structure, it has been known that the magnetic moment for the optimized structure is much smaller than the experimental value within the local density approximation²⁸. On the other hand, for the experimental structure, the size of magnetic moment is similar to that in the experiment ($\sim 1\mu_B$). In fact, within our calculations, the magnetic moment in FeGe decreases with decreasing the lattice constant as shown in Fig. 8 (a), which is consistent with previous studies^{24,29}. As a result, \tilde{D} exhibits non-trivial magnetic moment dependence as shown in Fig. 8 (b). Since the magnetic moment dependence of D is also an important issue, let us next discuss how the change in the lattice structure or the magnetic moment affect D in $\text{Mn}_{1-x}\text{Fe}_x\text{Ge}$. In Fig. 8 (c), we plot the lattice constant dependence of \tilde{D} , together with the distribution of band anti-crossings (d), (e) for lattice constants $a = 0.99a_0$ and $1.01a_0$, where a_0 is the experimental lattice constant. As can be seen, for larger a and magnetic moment, the energy difference of two peaks in the histogram of Fig. 3 becomes larger (Fig. 8(e)). Consequently, the density at which \tilde{D} changes its sign (n_c) becomes larger (Fig. 8(c)). However, the qualitative feature of \tilde{D} is robust against the change in a . Therefore, our calculation successfully explains why \tilde{D} is positive (negative) for MnGe (FeGe), and provides a useful guideline for materials design of skyrmion crystal in metallic helimagnets.

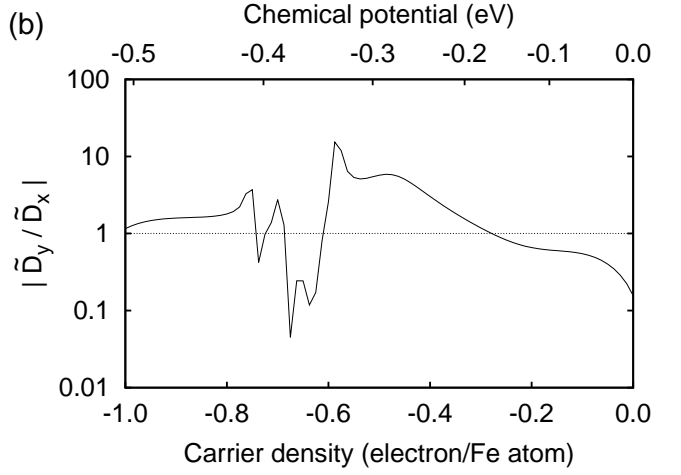
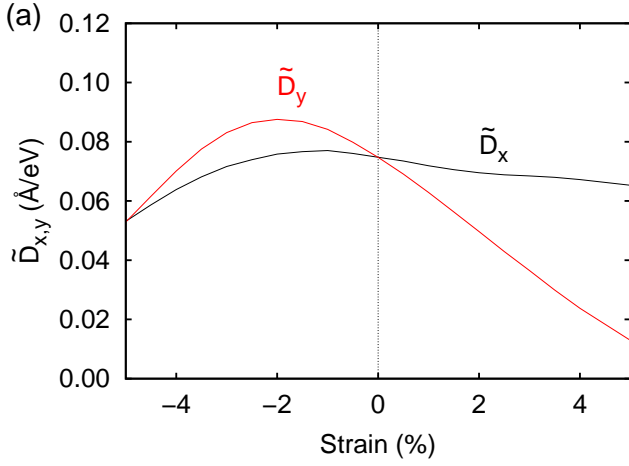


FIG. 6. **Strain dependence of the DM interaction.** (a) $\tilde{D}_{x,y}$ at $n = -0.45$ as a function of uniaxial strain along the y direction. (b) Anisotropy of the DM interaction, $|\tilde{D}_y/\tilde{D}_x|$ at +5% strain along the y direction as a function of the carrier density.

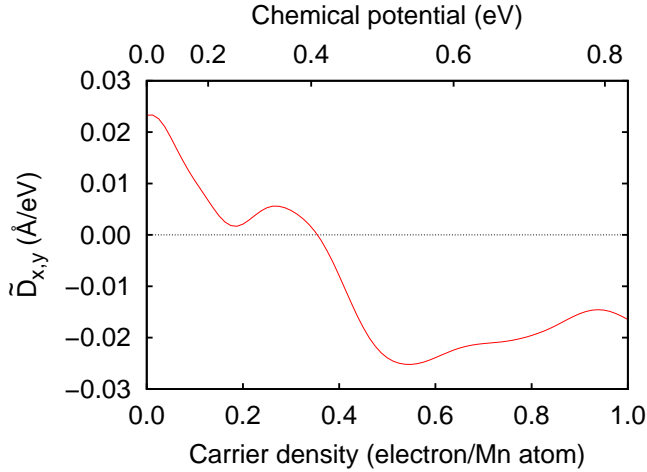


FIG. 7. **Carrier density dependence of the DM interaction starting from MnGe electronic structure.** Carrier density dependence of the DM interaction coefficients, \tilde{D}_x , and \tilde{D}_y . We use the electronic structure of MnGe ($n = 0.0$) for the same crystal structure as that of FeGe and employ the rigid band approximation. $n = 1.0$ ($\mu = 0.832$ eV) corresponds to the carrier density of FeGe.

TABLE I. **List of parameters for FeGe and MnGe.** Transition temperatures, T_N (K), ferromagnetic exchange couplings, J ($\text{meV}\text{\AA}^2$), helical periods, λ (\AA), experimental DM interactions evaluated by $D = 4\pi J/\lambda$ ($\text{meV}\text{\AA}$) and calculated D ($\text{meV}\text{\AA}$). J is evaluated by assuming $J \propto T_N$ and the values of $J = 52$ $\text{meV}\text{\AA}^2$ and $T_N = 30$ K for MnSi.

	T_N (K)	J ($\text{meV}\text{\AA}^2$)	λ (\AA)	D (expt.) ($\text{meV}\text{\AA}$)	D (calc.) ($\text{meV}\text{\AA}$)
FeGe	278	482	700	-8.7	-10.1
MnGe	170	295	30	124	107

Finally, let us compare the quantitative values of \tilde{D} with experiments. For this purpose, we should rescale \tilde{D} using the exchange splitting as $D = \Delta^2 \tilde{D}^{20}$. Using $\Delta = 1.17$ eV for FeGe and $\Delta = 2.14$ eV for MnGe based on the calculation shown in Fig. 7, we can obtain $D = -10.1$ $\text{meV}\text{\AA}$ for FeGe and $D = 107$ $\text{meV}\text{\AA}$ for MnGe. The experimental values of D can be estimated using J and the helical period, λ as $D = 4\pi J/\lambda$. Assuming that J scales to T_N and using the values of $J = 52$ $\text{meV}\text{\AA}^2$ and $T_N = 30$ K for MnSi^{18,30}, the experimental values of D for FeGe and MnGe are -8.7 $\text{meV}\text{\AA}$ and 124 $\text{meV}\text{\AA}$, respectively, which are in good agreement with our results (see Table I).

Method

Crystal structure. In the calculations, experimental values are used for the crystallographic parameters³¹. For the pressure and strain calculations, internal coordinates of the atoms are fixed and only the lattice parameters are modified. To symmetrize \tilde{D}_x and \tilde{D}_y , we use two different internal coordinates of atoms in the (4a) position, that is, (x, x, x) where $x_{\text{Fe,Mn}} = 0.135$ and $x_{\text{Ge}} = 0.842$, and the one with its 90-degree rotation along the z -axis and take the average. Note that our structure is right-handed according to Ref. 7. In the experiment, observed skyrmions on the right-handed crystal structure in FeGe (MnGe) are anticlockwise (clockwise), indicating that $D_{x,y} < 0$ ($D_{x,y} > 0$).

DFT calculations. To evaluate $\chi_0^{\alpha\beta}$ in FeGe, we perform the electronic structure calculation within the generalized-gradient approximation (GGA)³² based on the density functional theory³³. We use ultrasoft pseudopotentials³⁴ and plain-wave basis sets to describe the charge densities and wave functions with cutoff energies of 40Ry and 500Ry, respectively. We use $8 \times 8 \times 8$ k -point mesh. With including the spin-orbit couplings and assuming the ferromagnetic moment along the z axis, we obtain non-collinear magnetic structure. Using this electronic structure, we calculate Wan-

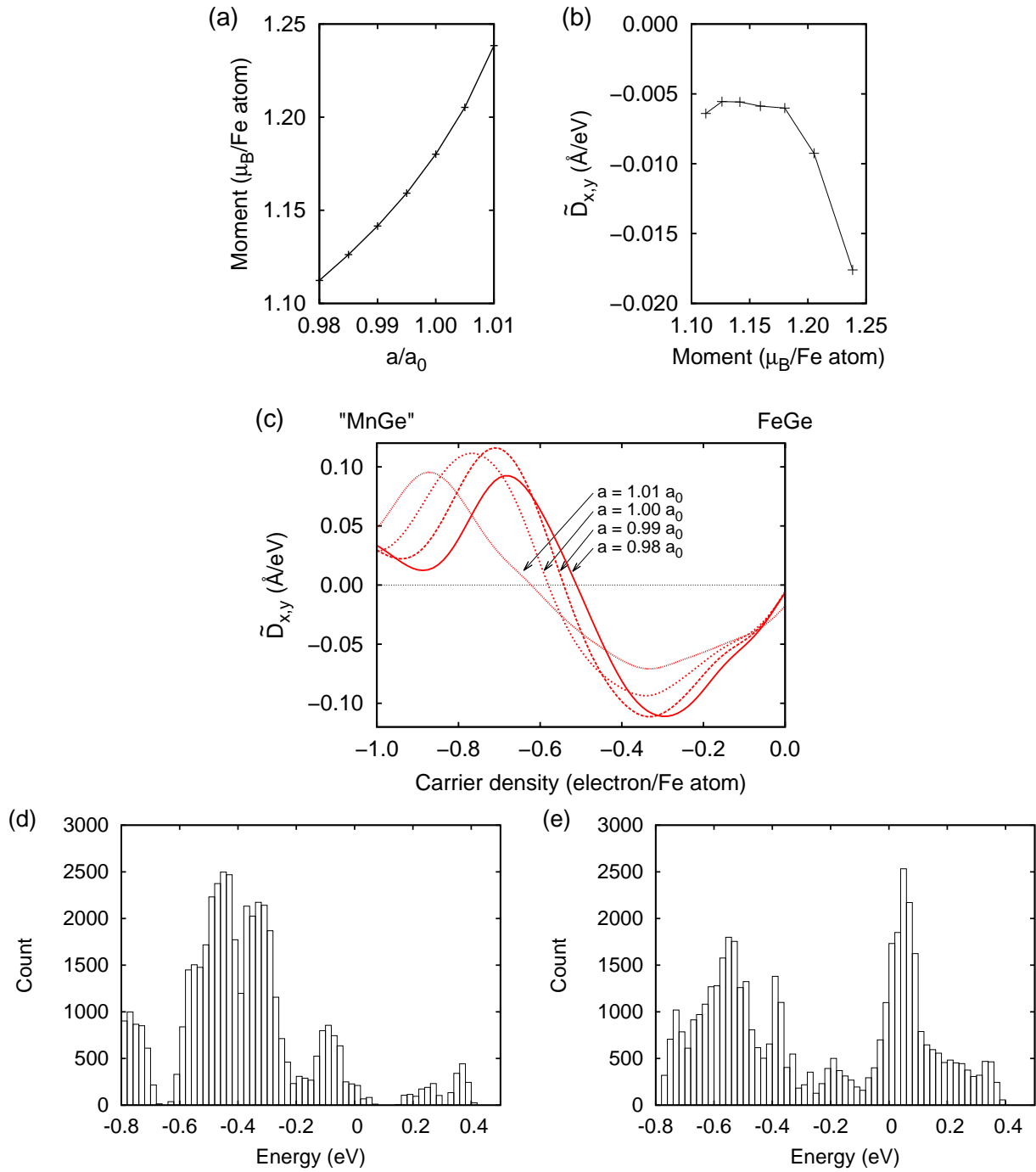


FIG. 8. **Lattice constant dependence of the DM interaction.** (a) Lattice constant dependence of the magnetic moment on each Fe atom for FeGe and (b) corresponding magnetic moment dependence of $\tilde{D}_{x,y}$. (c) $\tilde{D}_{x,y}$ with several lattice constants, $a/a_0 = 0.98, 0.99, 1.00$, and 1.01 . Distribution of anticrossing points at (d) $a/a_0 = 0.99$, and (e) $a/a_0 = 1.01$.

nier functions for Fe 3d and Ge 4p orbitals using wannier90 code^{35–37}. Based on the Wannier functions, we construct a tight-binding model on the restricted Hilbert space and calculate $\chi^{\alpha\beta}$ using $64 \times 64 \times 64$ k-point mesh at $T = 300\text{K}$.

The AHC is also calculated using the Wannier interpolation technique with $200 \times 200 \times 200$ k-point mesh³⁸.

- ¹ Bogdanov, A. N. & Yablonskii, D. A. Thermodynamically stable “vortices” in magnetically ordered crystals. The mixed state of magnets. *Sov. Phys. JETP* **68**, 101–103 (1989).
- ² Rößler, U. K., Bogdanov, A. N. & Pflöderer, C. Spontaneous skyrmion ground states in magnetic metals. *Nature* **442**, 797–801 (2006).
- ³ Mühlbauer, S. *et al.* Skyrmion Lattice in a Chiral Magnet. *Science* **323**, 915–919 (2009).
- ⁴ Yu, X. Z. *et al.* Real-space observation of a two-dimensional skyrmion crystal. *Nature* **465**, 901–904 (2010).
- ⁵ Yu, X. Z. *et al.* Near room-temperature formation of a skyrmion crystal in thin-films of the helimagnet FeGe. *Nature Materials* **10**, 106–109 (2011).
- ⁶ Nagaosa, N. & Tokura, Y. Topological properties and dynamics of magnetic skyrmions. *Nature Nanotech.* **8**, 899–911 (2013).
- ⁷ Shibata, K. *et al.* Towards control of the size and helicity of skyrmions in helimagnetic alloys by spin-orbit coupling. *Nature Nanotech.* **8**, 723–728 (2013).
- ⁸ Grigoriev, S. V. *et al.* Chiral Properties of Structure and Magnetism in $Mn_{1-x}Fe_xGe$ Compounds: When the Left and the Right are Fighting, Who Wins? . *Phys. Rev. Lett.* **110**, 207201 (2013).
- ⁹ Seki, S., Yu, X. Z., Ishiwata, S. & Tokura, Y. Observation of Skyrmions in a Multiferroic Material. *Science* **336**, 198 (2012).
- ¹⁰ Janson, O. *et al.* The quantum nature of skyrmions and half-skyrmions in Cu_2OSeO_3 . *Nature Communications* **5**, 1–11 (2014).
- ¹¹ Heide, M., Bihlmayer, G. & Blügel, S. Dzyaloshinskii-Moriya interaction accounting for the orientation of magnetic domains in ultrathin films: Fe/W(110). *Phys. Rev. B* **78**, 140403 (2008).
- ¹² Ferriani, P. *et al.* Atomic-Scale Spin Spiral with a Unique Rotational Sense: Mn Monolayer on W(001). *Phys. Rev. Lett.* **101**, 027201 (2008).
- ¹³ Heide, M., Bihlmayer, G. & Blügel, S. Describing Dzyaloshinskii-Moriya spirals from first principles. *Physica B: Phys. Cond. Matt.* **404**, 2678–2683 (2009).
- ¹⁴ Udvardi, L., Szunyogh, L., Palotás, K. & Weinberger, P. First-principles relativistic study of spin waves in thin magnetic films. *Phys. Rev. B* **68**, 104436 (2003).
- ¹⁵ Ebert, H. & Mankovsky, S. Anisotropic exchange coupling in diluted magnetic semiconductors: Ab initio spin-density functional theory. *Phys. Rev. B* **79**, 045209 (2009).
- ¹⁶ Katsnelson, M. I., Kvashnin, Y. O., Mazurenko, V. V. & Lichtenstein, A. I. Correlated band theory of spin and orbital contributions to Dzyaloshinskii-Moriya interactions. *Phys. Rev. B* **82**, 100403 (2010).
- ¹⁷ Dmitrienko, V. E. *et al.* Measuring the Dzyaloshinskii-Moriya interaction in a weak ferromagnet. *Nature Physics* **10**, 202–206 (2014).
- ¹⁸ Freimuth, F., Bamler, R., Mokrousov, Y. & Rosch, A. Phase-space Berry phases in chiral magnets: Dzyaloshinskii-Moriya interaction and the charge of skyrmions. *Phys. Rev. B* **88**, 214409 (2013).
- ¹⁹ Freimuth, F., Blügel, S. & Mokrousov, Y. Berry phase theory of Dzyaloshinskii-Moriya interaction and spin-orbit torques. *J. Phys.-Cond. Matt.* **26**, 104202 (2014).
- ²⁰ Wakatsuki, R., Ezawa, M. & Nagaosa, N. Domain wall of a ferromagnet on a three-dimensional topological insulator. ArXiv:1412.7910.
- ²¹ Nagaosa, N., Sinova, J., Onoda, S., MacDonald, A. H. & Ong, N. P. Anomalous Hall effect. *Rev. Mod. Phys.* **82**, 1539–1592 (2010).
- ²² Wäppling, R. & Haggström, L. Mossbauer study of cubic FeGe. *Phys. Lett. A* **28A**, 173 (1968).
- ²³ Lundgren, L., Blom, K. A. & Beckman, O. Magnetic susceptibility measurements on cubic FeGe. *Phys. Lett. A* **28A**, 175 (1968).
- ²⁴ Yamada, H., Terao, K., Ohta, H. & Kulatov, E. Electronic structure and magnetism of FeGe with B20-type structure. *Physica B* **329-333**, 1131–1133 (2003).
- ²⁵ Fang, Z. *et al.* The Anomalous Hall Effect and Magnetic Monopoles in Momentum Space. *Science* **302**, 92–95 (2003).
- ²⁶ Kanazawa, N. *et al.* Large Topological Hall Effect in a Short-Period Helimagnet MnGe. *Phys. Rev. Lett.* **106**, 156603 (2011).
- ²⁷ Kanazawa, N. Charge and heat transport phenomena in electronic and spin structures in B20-type compounds (2014). PhD thesis, Univ. of Tokyo.
- ²⁸ Neef, M., Doll, K. & Zwicky, G. Ab initio study of pressure-induced metal-insulator transition in cubic FeGe. *Phys. Rev. B* **80**, 035122 (2009).
- ²⁹ Jarlborg, T. Electronic structure and magnetism from supercell calculations. *Journal of Magnetism and Magnetic Materials* **283**, 238–246 (2004).
- ³⁰ Ishikawa, Y., Shirane, G., Tarvin, J. A. & Kohgi, M. Magnetic excitations in the weak itinerant ferromagnet MnSi. *Phys. Rev. B* **16**, 4956 (1977).
- ³¹ Lebeck, B., Bernhard, J. & Freltoft, T. Magnetic structures of cubic FeGe studied by small-angle neutron scattering. *J. Phys. Cond. Matt.* **1**, 6105–6122 (1989).
- ³² Perdew, J. P., Burke, K. & Ernzerhof, M. Generalized Gradient Approximation Made Simple. *Phys. Rev. Lett.* **77**, 3865 (1996).
- ³³ Giannozzi, P. *et al.* QUANTUM ESPRESSO: a modular and open-source software project for quantum simulations of materials. *J. Phys. Condens. Matter* **21**, 395502 (2009).
- ³⁴ Vanderbilt, D. Soft self-consistent pseudopotentials in a generalized eigenvalue formalism. *Phys. Rev. B* **41**, 7892 (1990).
- ³⁵ Marzari, N. & Vanderbilt, D. Maximally localized generalized Wannier functions for composite energy bands. *Phys. Rev. B* **56**, 12847–12865 (1997).
- ³⁶ Souza, I., Marzari, N. & Vanderbilt, D. Maximally localized Wannier functions for entangled energy bands. *Phys. Rev. B* **65**, 035109 (2001).
- ³⁷ Mostofi, A. A. *et al.* wannier90: A tool for obtaining maximally-localised Wannier functions. *Comp. Phys. Comm.* **178**, 685–699 (2008).
- ³⁸ Wang, X., Yates, J., Souza, I. & Vanderbilt, D. Ab initio calculation of the anomalous Hall conductivity by Wannier interpolation. *Phys. Rev. B* **74**, 195118 (2006).

Acknowledgements

The authors thank N. Kanazawa, W. Koshibae, D. Morikawa, K. Shibata, and Y. Tokura for helpful discussions. This work is supported by Grant-in-Aids for Scientific Research (No. 24224009 and No. 25104711) from the Ministry of Education, Culture, Sports, Science and Technology (MEXT) of Japan, and ImPACT Program of Council for Science, Technology and Innovation (Cabinet Office, Government of Japan).

Author contributions

T.K. carried out the numerical calculations. T.K., N.N. and R.A. analyzed the results and wrote the paper.